Nanoscale

PAPER

View Article Online
View Journal | View Issue

Cite this: *Nanoscale*, 2026, **18**, 10958

Bio-modified hydrogels in electrolyte-gated organic field-effect transistors for sensing applications

María Jesús Ortiz-Aguayo, [a] Sara Ruiz-Molina,[a] Carme Martínez-Domingo*†[a] and Marta Mas-Torrent *[a,b]

Received 6th February 2026,
Accepted 25th March 2026

DOI: 10.1039/d6nr00527f

rsc.li/nanoscale

Electrolyte – Gated Organic Field – Effect Transistors (EGOFETs) have attracted considerable interest as electrical transducers due to their low power consumption and strong potential for label – free biosensing. Hydrogels – polymeric networks capable of absorbing and retaining large amounts of water – have emerged as effective solid electrolyte media, enabling the replacement of liquid electrolytes in EGOFETs to form hydrogel-gated OFETs (HYGOFETs). In this work, we demonstrate the use of HYGOFETs for biosensing applications by employing agarose hydrogels functionalized with avidin as the solid electrolyte. The devices were integrated into a lateral flow system, and their electrical response to biotin was systematically investigated under continuous analysis. The bio-recognition event induced a measurable change in device capacitance, allowing the achievement of a very low limit of detection in the fM range. This study highlights the relevance of bio-compatible solid electrolytes for advancing robust, integrated, and physiologically compatible organic bio-sensing platforms.

1 Introduction

Electrolyte-gated organic field-effect transistors (EGOFETs) are attracting significant interest for the development of low-power electronic devices (typically operating below 1 V).[1] The EGOFET architecture relies on the replacement of the conventional dielectric layer of an organic field-effect transistor with an electrolyte medium, which is in direct contact with the organic semiconductor (OSC). The application of a gate–source voltage leads to the formation of electrical double layers at the OSC/electrolyte and electrolyte/gate interfaces, which are responsible for the OSC transport modulation.[2,3] In recent years, these devices have attracted significant attention as electronic transducers for biosensing applications, particularly when operated with aqueous electrolytes.[4–8] Nevertheless, alternative strategies based on the use of solid electrolytes are gaining increasing interest, as they enable low-voltage operation while providing enhanced device robustness.[9–13] Hydrogels are three-dimensional, cross-linked polymer networks that can absorb and retain large amounts of water while maintaining its structural integrity.[14] In addition, hydrogels show flexibility,[15] tuneable mechanical strength[16,17] and excellent biocompatibility.[18] These materials have been widely exploited for applications such as sensors,[19–22] touch panels,[23,24] energy storage systems,[25,26] drug delivery,[27,28] heavy metal ion removal,[29,30] contact lenses[31,32] and tissue engineering scaffolds,[33] among others.

Owing to their high-water content, hydrogels exhibit ultra-high capacitance values (on the order of μF cm^{-2}). Consequently, hydrogels can function as gel electrolytes in EGOFETs, overcoming the limitations of liquid water-based media and enabling efficient charge accumulation and carrier density modulation at very low voltages.[34–36] Hydrogel-gated-OFETs (HYGOFETs) have also been explored as pressure sensors.[12] In addition, a few studies have demonstrated the use of HYGOFETs for bio-sensing applications, such as the detection of pH variations, redox reactions, or the encapsulation of bio-chemical reactions.[37–40] It is well-established that hydrogels can be readily bio-functionalised,[41–43] and that analyte/bio-receptor interactions may alter the material properties, for example by inducing volumetric changes within the hydrogel.[44] However, to the best of our knowledge, bio-functionalised hydrogels have not yet been employed in HYGOFET architectures for bio-sensing applications. This work focuses on the production of bio-functionalized agarose hydrogel films and their integration in EGOFETs for sensing applications. As a model system, avidin-modified agarose was employed to detect biotin, exploiting the well-known high affinity and specificity avidin–biotin supramolecular complex.[45] First, a protocol was developed to obtain robust and optimised

[a]*Institut de Ciència de Materials de Barcelona, ICMAB-CSIC, Campus UAB, 08193 Bellaterra, Spain. E-mail: carme.martinez@imb-cnm.csic.es, mmas@icmab.es*
[b]*CIBER-BBN, Campus UAB, 08193 Bellaterra, Spain*
†Current address: Institut de Microelectrònica de Barcelona, IMB-CNM (CSIC), Campus UAB, 08193 Bellaterra, Spain.

hydrogel films, and the resulting HYGOFETs were electrically characterised. Subsequently, the devices were assembled by integrating a lateral flow (LF) nitrocellulose paper strip into the HYGOFET architecture (LF-HYGOFET), yielding a portable system that enables sample transport *via* the capillarity action of nitrocellulose and allows continuous analyte flow. Further, this approach eliminates the need to remove the hydrogel for *ex situ* analyte incubation, thereby simplifying the device operation and enhancing the transducer stability. The devices exhibited a linear response over a wide range of biotin concentrations, which was attributed to changes in the hydrogel capacitance, with a limit of detection in the fM range. Thus, this work demonstrates the feasibility of using bio-functionalised hydrogels for the development of reliable and efficient point-of-care diagnostics tools and sensors.

2 Results and discussion

The HYGOFET device configuration used is shown in Fig. 1a. Interdigitated gold source (S) and drain (D) electrodes as well as a coplanar gate (G) contact were fabricated on Kapton substrates. As active layer, a highly crystalline thin film of the OSC 2,8-difluoro-5,11 bis(triethylsilylethynyl)anthradithiophene (diF-TES-ADT) blended with polystyrene (PS) was prepared using the bar-assisted meniscus shearing (BAMS) technique, as previously reported (Fig. 1b).[8,12,46] To fabricate the hydrogel electrolyte matrices, a commercial avidin–modified agarose suspension was employed. Before use, the hydrogel was pretreated as described in the Experimental section. Briefly, 1 mL of commercial 6% avidin–agarose in an aqueous glycerol suspension was washed by centrifugation to remove glycerol (Fig. S1a and Experimental section). After this treatment, 0.5 mL of a solid packed gel was obtained, containing approximately 60 mg of avidin–agarose. Since avidin–agarose hydrogels alone did not yield mechanically robust and easily handled hydrogels, avidin–agarose was blended with a solution of non-modified agarose 2 wt% in water to obtain the following weight ratios avidin–agarose : agarose (1 : 0.33, 1 : 0.5 and 1 : 0.66) (Fig. S1b). To perform this task, the corresponding volumes of the non-modified agarose solution were directly added to the obtained 0.5 mL avidin–agarose hydrogel. In addition, as control, non-modified agarose hydrogel was also prepared (*i.e.*, ratio 0 : 1). Avidin–agarose : agarose hydrogels were prepared by drop casting hot solutions (60 °C) on a square polydimethylsiloxane (PDMS) gasket of 1 cm^2 placed on top of a glass slide, and letting the solution to cool down at room temperature. This process resulted in hydrogel films of approximately 3 mm thick. Afterwards, the hydrogel was removed from the substrate and placed on top of the OSC thin film and the gate area.

The devices were then electrically characterised. Agarose HYGOFETs, as previously reported, exhibit a slightly lower product of charge carrier mobility and electrical double-layer capacitance ($\mu \cdot C_{dl}$) and transconductance (g_m) values in comparison with devices measured in water (Fig. S2).[12] This was attributed to a lower effective concentration of mobile ions within the hydrogel, originating from the entrapped aqueous phase, as well as to reduced ion diffusion caused by steric constraints and interactions with the polymer network, ultimately diminishing their ability to modulate the HYGOFET channel conductivity. Fig. 1c displays the transfer characteristics in

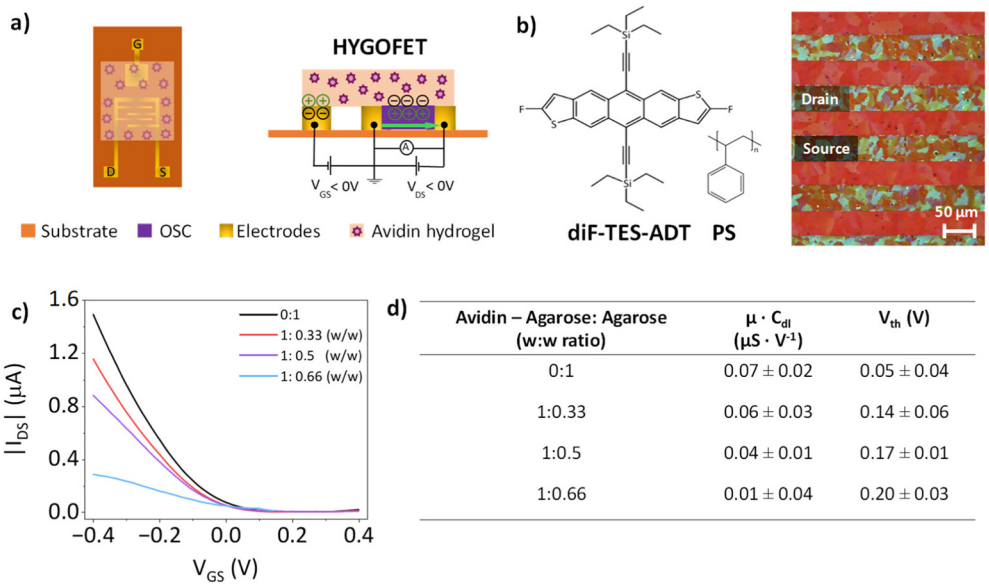

Avidin – Agarose: Agarose (w:w ratio)	$\mu \cdot C_{dl}$ ($\mu S \cdot V^{-1}$)	V_{th} (V)
0:1	0.07 ± 0.02	0.05 ± 0.04
1:0.33	0.06 ± 0.03	0.14 ± 0.06
1:0.5	0.04 ± 0.01	0.17 ± 0.01
1:0.66	0.01 ± 0.04	0.20 ± 0.03

Fig. 1 (a) Schematic representation of a hydrogel-gated organic field-effect transistor. (b) Molecular structure of diF-TES-ADT and PS, and polarized optical microscopy image of a diF-TES-ADT : PS thin film coated on a Kapton substrate with prefabricated interdigitated electrodes. (c) Transfer characteristics of the HYGOFETs using the 0 : 1, 1 : 0.33, 1 : 0.5, 1 : 0.66 (w : w) avidin–agarose : agarose ratios in linear regime (V_{DS} = −0.1 V). (d) Comparison of $\mu \cdot C_{dl}$ and V_{th} extracted from HYGOFETs in linear regime (N = 3) using hydrogels with different avidin–agarose : agarose ratios.

linear regime of the HYGOFETs based on hydrogels prepared from the different avidin–agarose : agarose ratios together with the response of an HYGOFET based on non-modified agarose for comparison. The extracted $\mu \cdot C_{dl}$ and threshold voltage (V_{th}) parameters obtained are summarised in Fig. 1d. The device performance exhibited a slight decrease in $\mu \cdot C_{dl}$ in the HYGOFETs based on agarose–avidin : agarose 1 : 0.33 and 1 : 0.5 compared to those based on non-modified agarose, which became more evident in the 1 : 0.66 mixture. Again, this is likely due to a reduced ion concentration and mobility within the matrix. Regarding the V_{th}, an increase was progressively observed with increasing the proportion of modified agarose. Based on these observations, the 1 : 0.33 ratio was selected as the optimal hydrogel composition for sensing measurements, as it provided the best electrical performance while maximizing the concentration of avidin moieties within the hydrogel.

To proceed with the sensing experiments, a nitrocellulose lateral flow (LF) paper strip was integrated into the HYGOFET, resulting in LF-HYGOFET devices (Fig. S3). We have shown very recently that the combination of EGOFETs with LF assays is a very appealing approach to develop point-of-care sensors, where the nitrocellulose can serve to transport the sample to analyse.[47] Additionally, the incorporation of nitrocellulose strip onto the hydrogel enables the continuous supply of the aqueous media into the HYGOFET, avoiding hydrogel dehydration and achieving a stable electrical performance over time (Fig. S4). Firstly, the nitrocellulose strip was treated with bovine serum albumin (BSA) to prevent unspecific biomolecule adsorption[48] and then positioned on top of the hydrogel of the HYGOFET, together with a sample pad (SP) and an absorbent pad (AP) at each end of the paper. Prior to biotin detection, the LF-HYGOFET was electrically conditioned to achieve a stable current response (see Experimental section). Subsequently, a reference transfer characteristic curve of the device was recorded using phosphate buffered saline solution (PBS 0.1 M, pH 7.4). Following, a volume of 200 μL of biotin solutions in PBS 0.1 M (pH 7.4) with concentrations ranging from 10^{-17} to 10^{-10} M were sequentially introduced in the sample pad, starting from the lowest to the highest concentration. It should be noted that this solution volume was previously optimized to ensure complete diffusion of the sample toward the device interfaces. After flowing each sample, the device was allowed to incubate for 15 minutes followed by a rinsing step. Then, the device transfer characteristic was recorded. This procedure was repeated for each tested concentration. Fig. 2a schematically illustrates the experimental protocol followed. The operation mechanism of an HYGOFET is governed by the formation of electrical double layers at the OSC/electrolyte and gate/electrolyte interfaces, where most of the voltage drop takes place. Thus, the interfacial layer near the device interfaces with the hydrogel (typically on the order of a few angstroms to few nanometres) is expected to effectively contribute to the sensing mechanism (Fig. 2b).

Fig. 3a shows the transfer characteristics obtained upon the exposure of the LF-HYGOFET to each biotin concentration. It can be observed that source–drain current (I_{DS}) decreases while increasing biotin concentration. Electrical variations resulting from the bio-recognition process were assessed by calculating the change in current intensity ($\Delta I = I_{DS} - I_{DS,0}$) at a source–gate voltage (V_{GS}) −0.4 V, where I_{DS} represents the source–drain current measured at a given antigen concentration, and $I_{DS,0}$ corresponds to the value prior to biotin exposure. Calibration curves, obtained by plotting the normalized ΔI against biotin concentration, are presented in Fig. 3b. A lineal response is observed in the concentration range from 10^{-15} to 10^{-11} M. In this region, the data could be fitted giving

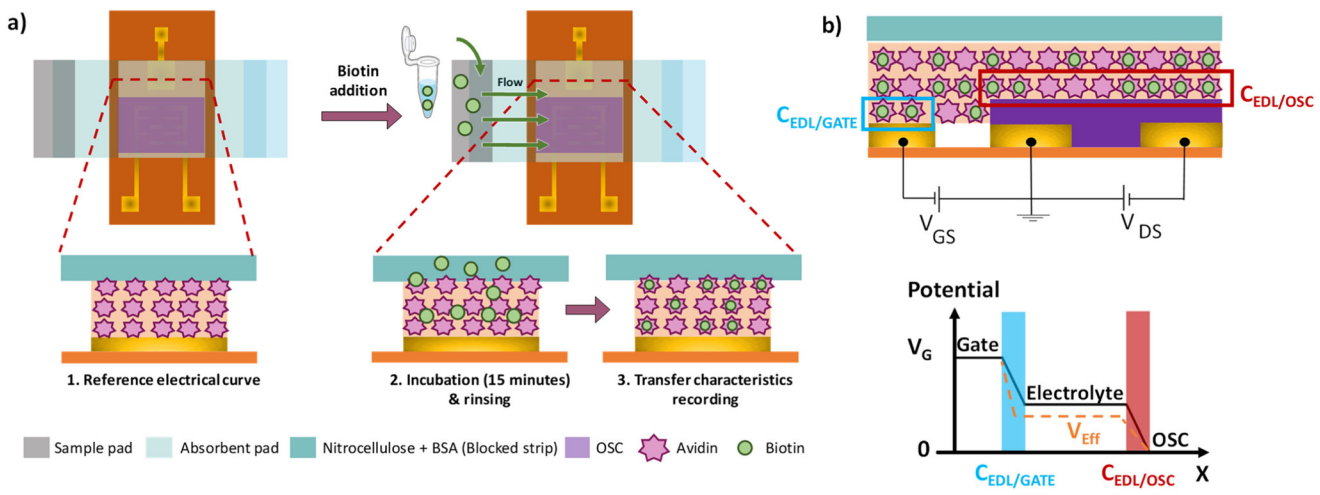

Fig. 2 (a) Schematic representation of a LF-HYGOFET device, in which a nitrocellulose paper with a sample pad and an absorbing pad is assembled on the transistor. The sensing experiment consists in introducing biotin solutions in PBS, followed by an incubation period of 15 minutes, a rinsing step with PBS and, finally, the recording of the device transfer characteristics. In this process, the complex avidin–biotin is formed within the hydrogel, altering the device electrical characteristics. (b) HYGOFET scheme illustrating the gate potential drop at the hydrogel/gate and hydrogel/OSC interfaces. Only the biorecognition events occurring at these interfaces are responsible for the observed changes in the electrical double-layer capacitances (dotted orange line).

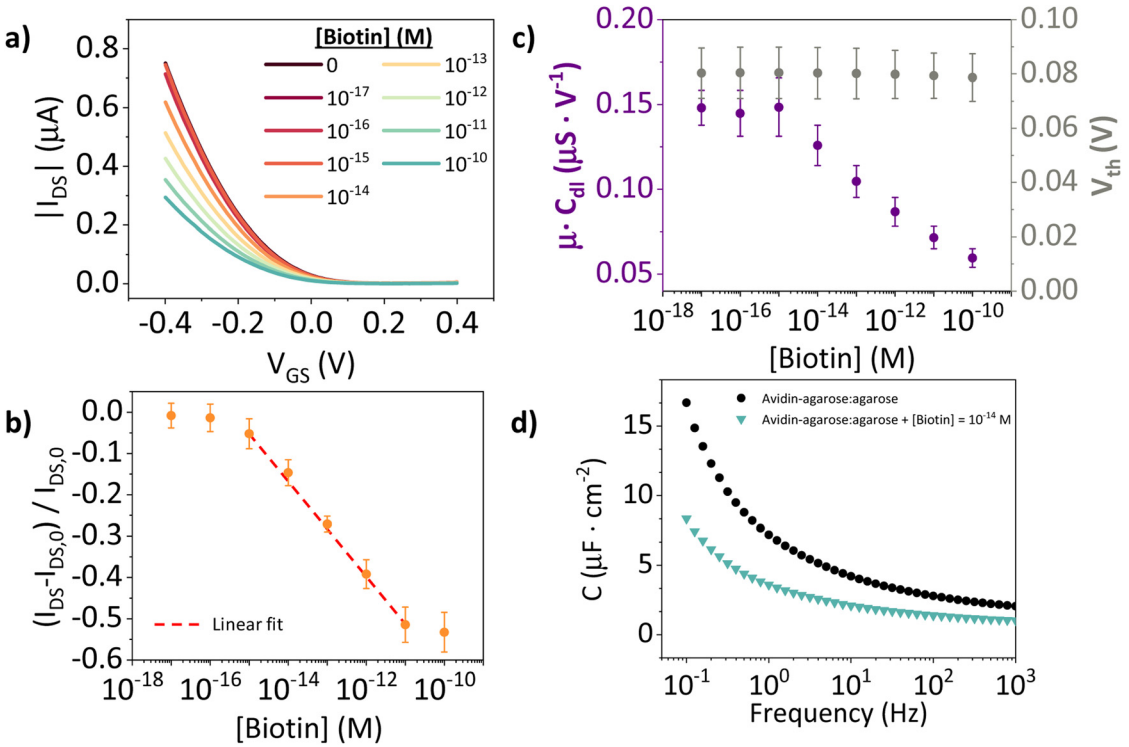

Fig. 3 (a) Transfer characteristics of HYGOFETs based on avidin-modified agarose embedded in the lateral flow assay system and exposed to an increasing concentration of biotin (V_{DS} = −0.1 V and V_{GS} = from 0.4 V to −0.4 V). (b) Representation of $(I_{DS} - I_{DS,0})/I_{DS,0}$ extracted from the transfer characteristics at V_{GS} = −0.4 V for N = 3 devices. (c) $\mu{\cdot}C_{dl}$ and V_{th} *vs.* biotin concentration for N = 3 devices. (d) Capacitance measurements extracted from avidin–agarose : agarose (1 : 0.33) hydrogels sandwiched between two gold electrodes before and after exposure to a biotin solution (10^{-14} M) in PBS.

a slope of 0.05 ± 0.01 M^{-1} (r^2 = 0.997) corresponding to the device sensitivity. Further, a low limit of detection (LOD) of 5.1 fM was extracted (see Experimental section).

In EGOFETs, the product $\mu{\cdot}C_{dl}$ represents the effective transconductance factor, where μ denotes the OSC charge-carrier mobility and C_{dl} stands for the interfacial electrical double layer capacitance and quantifies the interfacial charge accumulation at device interfaces, which is responsible for the channel conductivity modulation. When EGOFETs are deployed for biosensing, a binding recognition event can induce different electrical responses depending on the dominant underlying mechanism.[49] If the binding event affects the charge carrier mobility or the device capacitance, a change in the slope of the transfer curve is expected. In contrast, when the interaction primarily alters the metal work function (potentiometric effect), a lateral shift of the transfer curve is observed, manifested as a V_{th} shift.[3,50,51] In our experiments, the sensing response leads to a reduction of the $\mu{\cdot}C_{dl}$, whilst V_{th} remains essentially unchanged (Fig. 3c). Thus, the sensing mechanism is primarily governed by a capacitive effect. As the hydrogel is exposed to a higher concentration of biotin, more avidin binding sites from the hydrogel become occupied, forming avidin–biotin complexes.[45,52,53] The avidin–biotin binding event occurs throughout the hydrogel, but its electrical effect on the HYGOFET is strictly interfacial (Fig. 2b). Since the device response is governed by the electrical double layer within the Debye length, only recognition events near this region can modulate the effective capacitance, regardless of hydrogel thickness.[54] The bio-recognition event might introduce conformational changes in the structure of the agarose hydrogel, as well as alter the charge distribution within the gel. In fact, avidin is positively charged at neutral pH, when it binds to biotin the net positive charge is reduced and the ionic distribution modified, affecting the properties of the electrical double layers at the hydrogel-gate and hydrogel-OSC interfaces.[55]

To further confirm that the sensing mechanism is capacitive, Electrochemical Impedance Spectroscopy (EIS) was employed to measure the impedance as a function of frequency of the bio-functionalized agarose hydrogels, before and after biotin exposure (Fig. 3d). For this purpose, the avidin–agarose : agarose (1 : 0.33) hydrogel was exposed to a 10^{-14} M biotin solution in PBS. As it can be observed, upon addition of biotin, a clear decrease in capacitance was observed, consistent with the trend observed in the transfer characteristics. Capacitance values before and after the biotin exposure were extracted and normalised by area employing the formula described in the Experimental section (Table S1).

To ensure the specificity of the sensing platform and non-specific biomolecule adsorption, a control experiment was conducted by using an HYGOFET based on non-modi-

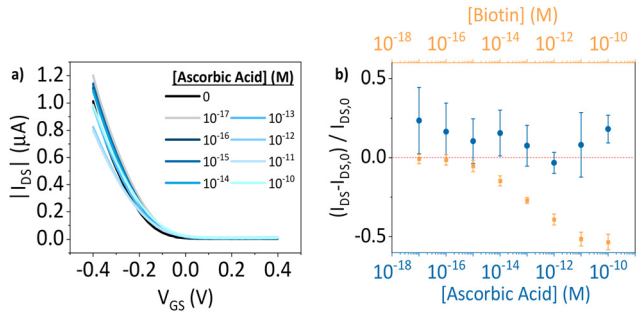

Fig. 4 (a) Transfer curves (V_{DS} = −0.1 V) of LF-HYGOFETs based on agarose–avidin : agarose (1 : 0.33) hydrogels exposed to solutions of acid ascorbic, as interferent, at different concentrations. (b) Relative current variation of the devices as a function of ascorbic acid and biotin concentrations (N = 6).

fied agarose and adding progressively increasing concentrations of the biotin solutions. The results indicate that the I_{DS} fluctuated randomly within a 10–20% range, with no systematic drift observed (Fig. S5). These results confirm that the I_{DS} response is due to the biotin–avidin recognition interaction.

To further examine potential cross-reactivity of the sensing mechanism, an additional experiment was carried out, in which the avidin–agarose : agarose (1 : 0.33) hydrogel-based LF-HYGOFET was exposed to increasing concentrations of ascorbic acid in PBS 0.1 M, a molecule chosen as a non-target interferent due to its chemical similarity to biotin.[56–59] The resulting transfer characteristics are plotted in Fig. 4a, showing no consistent trend in the measured I_{DS} with the exposition of the interferent (Fig. 4b). These findings provide additional evidence that the capacitive changes observed in the biotin sensing experiment are mainly attributed to the specific interaction of biotin with avidin.

3 Conclusions

In this study, agarose-based hydrogels were employed as an alternative to conventional liquid electrolytes in EGOFETs, leading to the development of HYGOFETs. Agarose was chosen as the hydrogel matrix due to its low cost, wide availability, and simple gelation process. To demonstrate the potential of these devices for biosensing applications, a receptor biomolecule, avidin, was incorporated into the hydrogel matrix. The sensing performance was investigated by integrating the HYGOFET with a lateral flow system, enabling continuous and real-time detection. The platform was validated through the detection of avidin–biotin interactions, which induced changes in the electrical double-layer capacitance and, consequently, in the measured source–drain current, achieving a very low limit of detection of ~5 fM.

These results show that HYGOFETs retain the key advantages of conventional EGOFETs, such as low operating voltage and compatibility with aqueous environments, while offering easier handling and simplified fabrication. Furthermore, we demonstrate that, through chemical modification of the hydrogel matrix, these devices can be effectively employed for highly sensitive bio-sensing applications. Importantly, the hydrogels used in this work are biocompatible and biodegradable, making the proposed platform particularly attractive for sustainable and bio-integrated sensing technologies.

4 Experimental section

4.1 Materials

Agarose powder (Type I–B, low EEO), polystyrene (M_w = 10 000 g mol^{-1}), anhydrous 99.8% chlorobenzene (CB), 2,3,4,5,6-pentafluorothiophenol (PFBT), Avidin–agarose from egg white – aqueous glycerol 50% suspension, Bovine Serum Albumin (BSA, M_w = 66 kDa), biotin (≥99%, HPLC) lyophilized powder and L-ascorbic acid (99%) were purchased from Sigma-Aldrich. Polydimethylsiloxane (PDMS), Qsil216 A/B for gasket production was purchased from Farnell Components. 2,8-Difluoro-5,11-bis(triethylsilylethynyl)anthradithiophene (diF TES-ADT, purity >99%) racemic mixture was purchased from Luminisence Technology Corp (LUMTEC). Acetone and isopropanol HPLC grade were purchased from Chem-Lab. All these commercial materials were used without any further purification. Kapton® foils, used as substrate, were bought from DuPont (Kapton®HN, 125 μm thick). Lateral flow components, unbacked nitrocellulose test membrane (AE98), sample and absorbent pads (CF4) were obtained from Cytiva Lifescience.

4.2 EGOFET manufacture

For EGOFET devices fabrication, interdigitated source (S), drain (D), and coplanar gate (G) electrodes were patterned on 125 μm thick Kapton foil substrates using positive photolithography (Micro-Writer ML2, Durham Magneto Optics Ltd). Metallization was carried out *via* thermal evaporation (System Auto 360, BOC Edwards), depositing a 5 nm chromium adhesion layer followed by a 40 nm gold layer. The resulting channel dimensions were 18 000 μm in width (W) and 50 μm in length (L), yielding a W/L ratio of 360. The area of the gate electrode was of 0.15 cm^2. The lift-off process was performed by sequential cleaning in acetone and isopropanol for 5 minutes each, repeated twice.

Prior to active layer deposition, the electrodes underwent ultrasonic cleaning in acetone and isopropanol. The organic semiconductor (OSC) deposition protocol followed previously reported procedures.[46] Briefly, the substrates with patterned gold electrodes were first exposed to UV-ozone for 25 minutes, then immersed in a 15 mM solution of PFBT in isopropanol for 15 minutes and rinsed. Subsequently, a 2 wt% solution of diF-TES-ADT and polystyrene (PS) in a 4 : 1 volume ratio, dissolved in CB, was deposited using the Bar-Assisted Meniscus Shearing (BAMS) technique.[46,54] The coating process was carried out at a shearing speed of 10 mm s^{-1} while maintaining the substrate temperature at 105 °C. Polarized optical microscopy (POM) images were acquired in reflection mode

using an Olympus BX51 microscope equipped with a polarizer and analyzer set at 90°.

4.3 Hydrogel preparation

Agarose 2 wt% solution. The agarose solution was prepared at 2 wt% by dissolving the agarose powder in MilliQ water (resistivity: 18.2 MΩ cm at 25 °C) under continuous stirring (800 rpm) at 120 °C for 5–10 minutes. Once the agarose solution became transparent, it was immediately used for the film preparation, as previously reported.[12]

Agarose films were prepared using the BAMS technique at a coating speed of 10 mm s^{-1} and keeping the plate temperature at 30 °C, close to the agarose jellification temperature. Before deposition, the tip of the micropipette was kept in hot agarose solution (120 °C) for some seconds to avoid the jellification inside the plastic tip. Upon cooling down to room temperature, the resulting agarose film was subsequently cut into square pieces (around 1 cm^2) and immediately used as electrolyte in the transistors by sandwiching it on top on the prepared devices.

Avidin–agarose : agarose solution. Commercial agarose–avidin hydrogel is delivered initially suspended in glycerol, which acts as stabilizing agent. To remove the glycerol, 1 mL of the agarose–avidin suspension was washed with 1× phosphate-buffered saline (PBS 0.1 M; pH = 7.4) in an Eppendorf tube, followed by centrifugation at 2000 rpm. The resulting supernatant was carefully discarded to eliminate residual glycerol. This washing step was repeated three additional times using 0.5 mL of PBS per wash. From each 1 mL of the original agarose suspension, approximately 0.5 mL of solid packed hydrogel was recovered. Since these gels are hard to manipulate, the suspensions were mixed with agarose. Therefore, agarose–avidin : agarose mixtures were prepared using the avidin : agarose packed gel obtained and adding different volumes (1, 1.5 and 2 ml) of the agarose suspension 2% (w/w) to obtain the following w/w mixture ratios: 1 : 0.33, 1 : 0.5 and 1 : 0.66. The mixtures were heated at 60 °C, to prevent avidin denaturalization, until a homogeneous solution was obtained. A polydimethylsiloxane (PDMS) gasket was employed for the formation of a gel with a specific area. Hence, the hot solutions (60 °C) were deposited on a square PDMS pool of 1 cm^2 and let to cool down at room temperature, leading to films 0.5 cm thick. To prevent dehydration of the gels, all the prepared hydrogels were stored in a refrigerator at 5 °C.

4.4 LF – HYGOFET assembly

The prepared hydrogel was deposited on top of the device ensuring covering the organic semiconductor channel and gate electrode. Before assembling the LF strip on the HYGOFET, 1 mL of a BSA solution in PBS (1 mg ml^{-1}) was deposited on the nitrocellulose strip and sample pad at let it react for 20 minutes at 37 °C in order to avoid unspecific absorption along the strip test. Afterwards, the LF strip paper was positioned on top of the hydrogel. At the edges of the nitrocellulose paper, a sample pad and an absorbent pad were placed, maintaining a 2 mm overlap on each side to ensure proper capillary flow. Since the absorbent pad does not directly influence or interfere with the device response, it was not treated with BSA.

4.5 LF – HYGOFET characterization

LF-HYGOFETs were electrically characterized under ambient conditions using a Keithley 2612A Source Meter controlled *via* a custom Phyton script. Initially, LF-HYGOFET devices were conditioned by applying a source–gate voltage (V_{GS}) of −0.1 V and a source–drain voltage (V_{DS}) of −0.1 V. This conditioning continued for approximately 30 minutes until the source–drain current (I_{DS}) stabilized. Once a steady-state was achieved, the initial transfer curve and output characteristics were recorded and used as a reference to assess device performance.

To monitor the electrical changes in performance induced by the sensing event, device figures of merit, including the threshold voltage (V_{th}) and the product of mobility (μ) and double-layer capacitance (C_{dl}), were derived from the slope (b) and y-intercept (a) of the linear fitting of each transfer characteristic using the following equations:

$$V_{th} = -\frac{a}{b} - \frac{V_{DS}}{2}$$

$$\mu \cdot C_{dl} = \frac{L}{W}\frac{b}{V_{DS}}$$

4.6 Sensing experiments

Sensing experiments were conducted using a single HYGOFET device integrated into a LF system. This setup enabled continuous operation and helped to prevent dehydration of the hydrogel. Initially, the device was conditioned by flowing 0.1 M a PBS solution (pH 7.4) through the nitrocellulose membrane to ensure proper hydration of the hydrogel. Once a steady-state drain–source current was achieved, 200 μL of biotin or interferent solutions at varying concentrations (ranging from 10^{-17} to 10^{-10} M) were applied dropwise onto the sample pad. After a 15-minute incubation period to allow complete interaction with the hydrogel, the membrane was rinsed. This rinsing step consisted of dispensing 200 μL of 0.1 M PBS onto the sample pad, allowing it to flow along the nitrocellulose strip by capillary action, in order to remove unbound or loosely adsorbed biomolecules from the nitrocellulose membrane. Following a 5-minute stabilization period, the electrical response of the LF-HYGOFET was recorded by measuring the transfer characteristics in the linear regime (V_{DS} = −0.1 V).

Sensitivity was determined by calculating the slope of the calibration curve. The limit of detection (LOD) has been calculated using the following equation:

$$\mathrm{LOD} = \frac{3.3 \cdot \sigma}{S}$$

where σ stands for deviation of the blank response and S for the slope of the calibration curve.

4.7 Capacitance measurements

The electrical double layer (EDL) capacitance values were obtained by employing the Electrochemical Impedance

Spectroscopy (EIS) technique. Measurements were carried out with Autolab potentiostat/galvanostat (PGSTAT128N). Setup measurements relied on the sandwiching the hydrogel in between two gold electrodes of 1 cm^2, which were connected to the potentiostat and used as working and auxiliary electrodes.

Impedance spectra (capacitance *vs.* frequency) were recorded at different DC bias potentials within the operational window of the HYGOFET, using a small-signal AC perturbation of 5 mV (V_{RMS}). Capacitance was obtained from the imaginary part of the impedance according to:

$$C = \frac{1}{2\pi f|Z''|}$$

where C is the capacitance, measured in Farads (F), f is the frequency of the applied AC signal measured in Hertz (Hz), and $|Z''|$ is the magnitude of the imaginary part of the impedance.

Author contributions

M. O.-A. and S. R.-M. performed the experimental work and the data analysis. C. M.-D. and M. M.-T. supervised the project. M. M-T. conceived the idea. M. O.-A, C. M.-D. and M. M.-T. co-wrote the manuscript.

Conflicts of interest

There are no conflicts to declare.

Data availability

The data published in this paper will be provided by the authors when requested.

Supplementary information (SI) is available. See DOI: https://doi.org/10.1039/d6nr00527f.

Acknowledgements

This work was funded by MCIN/AEI/10.13039/501100011033/ERDF, UE, with projects SENSATION PID2022-141393OB-I00 and PDC2021-121511-I00, and through the "Severo Ochoa" Programme for Centers of Excellence in R&D (CEX2023-001263-S). The authors also acknowledge funds from the Generalitat de Catalunya (2021-SGR-00443). S. R. acknowledges her FPI fellowship. S. R. and M. O. are enrolled at the UAB Chemistry PhD program. The authors thank Dr Dean Kos for software development.

References

1 L. Torsi, M. Magliulo, K. Manoli and G. Palazzo, Organic field-effect transistor sensors: a tutorial review, *Chem. Soc. Rev.*, 2013, **42**, 8612.
2 F. Torricelli, *et al.*, Electrolyte-gated transistors for enhanced performance bioelectronics, *Nat. Rev. Methods Primers*, 2021, **1**, 66.
3 L. Kergoat, *et al.*, Tuning the threshold voltage in electrolyte-gated organic field-effect transistors, *Proc. Natl. Acad. Sci. U. S. A.*, 2012, **109**, 8394–8399.
4 G. Y. Wang, K. Lian and T.-Y. Chu, Electrolyte-Gated Field Effect Transistors in Biological Sensing: A Survey of Electrolytes, *IEEE J. Electron Devices Soc.*, 2021, **9**, 939–950.
5 Y. Liang, *et al.*, Bioinspired Electrolyte-Gated Organic Synaptic Transistors: From Fundamental Requirements to Applications, *Nano-Micro Lett.*, 2025, **17**, 198.
6 S. K. Sailapu, *et al.*, Standalone operation of an EGOFET for ultra-sensitive detection of HIV, *Biosens. Bioelectron.*, 2020, **156**, 112103.
7 E. Macchia, *et al.*, Single-molecule detection with a millimetre-sized transistor, *Nat. Commun.*, 2018, **9**, 3223.
8 S. Ricci, *et al.*, Label-free immunodetection of α-synuclein by using a microfluidics coplanar electrolyte-gated organic field-effect transistor, *Biosens. Bioelectron.*, 2020, **167**, 112433.
9 Y. Zhong, *et al.*, Eutectogels as a Semisolid Electrolyte for Organic Electrochemical Transistors, *Chem. Mater.*, 2024, **36**, 1841–1854.
10 A. Alyami, M. Skowrons, K. Perera, B. Lüssem and A. Jákli, Performance of Organic Electrochemical Transistors with Ionic Liquid Crystal Elastomers as Solid Electrolytes, *ACS Appl. Mater. Interfaces*, 2024, **16**, 54282–54291.
11 B. Singh, R. A. Mishra and D. Punetha, Optimizing performance of electrolyte-gated organic field-effect transistors for biosensing: material variations and parameter analysis, *Discov. Electron.*, 2025, **2**, 20.
12 Q. Zhang, F. Leonardi, R. Pfattner and M. Mas-Torrent, A Solid–State Aqueous Electrolyte–Gated Field–Effect Transistor as a Low–Voltage Operation Pressure–Sensitive Platform, *Adv. Mater. Interfaces*, 2019, **6**, 1900719.
13 A. Miyamoto, *et al.*, Solid Electrolyte Gas Sensor Based on a Proton-Conducting Graphene Oxide Membrane, *ACS Omega*, 2017, **2**, 2994–3001.
14 F. Ullah, M. B. H. Othman, F. Javed, Z. Ahmad and H. M. Akil, Classification, processing and application of hydrogels: A review, *Mater. Sci. Eng., C*, 2015, **57**, 414–433.
15 *Nano Hydrogels: Physico-Chemical Properties and Recent Advances in Structural Designing*, Springer Singapore, Singapore, 2021. DOI: 10.1007/978-981-15-7138-1.
16 A. S. Maier, *et al.*, Cytocompatible Hydrogels with Tunable Mechanical Strength and Adjustable Swelling Properties through Photo-Cross-Linking of Poly(vinylphosphonates), *ACS Appl. Mater. Interfaces*, 2024, **16**, 58135–58147.
17 L. Fu and H. Li, Ionic Crosslinking Improves the Stiffness and Toughness of Protein Hydrogels, *Polym. Sci. Technol.*, 2025, **1**, 342–350.
18 M. M. H. Rumon, *et al.*, Progress in hydrogel toughening: addressing structural and crosslinking challenges for biomedical applications, *Discover Mater.*, 2025, **5**, 5.

19 D. Buenger, F. Topuz and J. Groll, Hydrogels in sensing applications, *Prog. Polym. Sci.*, 2012, **37**, 1678–1719.
20 Y. Lin, *et al.*, Recent progress of nanomaterials-based composite hydrogel sensors for human–machine interactions, *Discover Nano*, 2025, **20**, 60.
21 K. Nagamine, *et al.*, Noninvasive Sweat-Lactate Biosensor Emplsoying a Hydrogel-Based Touch Pad, *Sci. Rep.*, 2019, **9**, 10102.
22 T. Du, Z. Zhu, M. Chen, X. Yan and Y. Li, Functional Hydrogel Strain Sensors for Smart Electronic Devices: Strategies and Recent Progress, *ACS Appl. Electron. Mater.*, 2024, **6**(8), 5402–5428.
23 Y. Li, *et al.*, An ultrastretchable and multifunctional hydrophobic/electrostatic dual-crosslinked hydrogel for self-healing flexible touch panel and sensor, *npj Flexible Electron.*, 2025, **9**, 45.
24 T. Feng, *et al.*, Stretchable on-skin touchless screen sensor enabled by ionic hydrogel, *Nano Res.*, 2024, **17**, 4462–4470.
25 Z. Shen, *et al.*, Hydrogel Electrolytes-Based Rechargeable Zinc-Ion Batteries under Harsh Conditions, *Nano-Micro Lett.*, 2025, **17**, 227.
26 K. Sadaiyandy, *et al.*, A review on redox hydrogel electrolyte for energy storage devices, *Ionics*, 2025, **31**, 8837–8873.
27 H. Hameed, S. Faheem, A. C. Paiva-Santos, H. S. Sarwar and M. Jamshaid, A Comprehensive Review of Hydrogel-Based Drug Delivery Systems: Classification, Properties, Recent Trends, and Applications, *AAPS PharmSciTech*, 2024, **25**, 64.
28 M. Baghali, H. Ziyadi and A. Di Martino, Engineering smart hydrogels for intelligent drug delivery, *Polym. Bull.*, 2025, **82**, 2287–2328.
29 S. Lee, Y. Eom, J. Park, J. Lee and S. Y. Kim, Micro-hydrogel Particles Consisting of Hyperbranched Polyamidoamine for the Removal of Heavy Metal Ions from Water, *Sci. Rep.*, 2017, **7**, 10012.
30 D. Gokhale, A. F. Hamelberg and P. S. Doyle, Multifunctional zwitterionic hydrogels for the rapid elimination of organic and inorganic micropollutants from water, *Nat. Water*, 2024, **2**, 62–71.
31 M. Hisham, A. E. Salih and H. Butt, 3D Printing of Multimaterial Contact Lenses, *ACS Biomater. Sci. Eng.*, 2023, **9**, 4381–4391.
32 K. Ishihara, *et al.*, Biomimetic-Engineered Silicone Hydrogel Contact Lens Materials, *ACS Appl. Bio Mater.*, 2023, **6**, 3600–3616.
33 B. S. MohanKumar, *et al.*, Hydrogels: potential aid in tissue engineering—a review, *Polym. Bull.*, 2022, **79**, 7009–7039.
34 L. M. Dumitru, *et al.*, A hydrogel capsule as gate dielectric in flexible organic field-effect transistors, *APL Mater.*, 2015, **3**, 014904.
35 L. Fillaud, *et al.*, Switchable Hydrogel-Gated Organic Field-Effect Transistors, *Langmuir*, 2018, **34**, 3686–3693.
36 M. Azimi, A. Subramanian, J. Fan, F. Soavi and F. Cicoira, Electrical and mechanical stability of flexible, organic electrolyte-gated transistors based on iongel and hydrogels, *J. Mater. Chem. C*, 2023, **11**, 4623–4633.
37 G. Li, *et al.*, Acrylamide Hydrogel-Modified Silicon Nanowire Field-Effect Transistors for pH Sensing, *Nanomaterials*, 2022, **12**, 2070.
38 H. D. Chirra and J. Z. Hilt, Nanoscale Characterization of the Equilibrium and Kinetic Response of Hydrogel Structures, *Langmuir*, 2010, **26**, 11249–11257.
39 J. L. Gall, *et al.*, Algae-functionalized hydrogel-gated organic field-effect transistor. Application to the detection of herbicides, *Electrochim. Acta*, 2021, **372**, 137881.
40 J. Pallu, *et al.*, A DNA hydrogel gated organic field effect transistor, *Org. Electron.*, 2019, **75**, 105402.
41 F. Qu, Y. Zhang, A. Rasooly and M. Yang, Electrochemical Biosensing Platform Using Hydrogel Prepared from Ferrocene Modified Amino Acid as Highly Efficient Immobilization Matrix, *Anal. Chem.*, 2014, **86**, 973–976.
42 S. Hageneder, *et al.*, Responsive Hydrogel Binding Matrix for Dual Signal Amplification in Fluorescence Affinity Biosensors and Peptide Microarrays, *ACS Appl. Mater. Interfaces*, 2021, **13**, 27645–27655.
43 P. Shen, *et al.*, Aptamer-functionalized smart photonic hydrogels: application for the detection of thrombin in human serum, *NPG Asia Mater.*, 2022, **14**, 94.
44 K. Cherifi and S. Matoori, Hydrogels for Analyte Sensing, *ACS Meas. Sci. Au*, 2025, **5**(6), 771–779.
45 R. F. Delgadillo, *et al.*, Detailed characterization of the solution kinetics and thermodynamics of biotin, biocytin and HABA binding to avidin and streptavidin, *PLoS One*, 2019, **14**, e0204194.
46 I. Temiño, *et al.*, A Rapid, Low–Cost, and Scalable Technique for Printing State–of–the–Art Organic Field–Effect Transistors, *Adv. Mater. Technol.*, 2016, **1**, 1600090.
47 M. J. Ortiz-Aguayo, C. Martínez-Domingo, D. Gutiérrez, D. Kos and M. Mas-Torrent, Electrically Readable Lateral Flow Assay Using Organic Transistors for Diagnostic Applications, *Adv. Mater.*, 2025, e13468, DOI: 10.1002/adma.202513468.
48 X. Jiang and P. B. Lillehoj, Lateral flow immunochromatographic assay on a single piece of paper, *Analyst*, 2021, **146**, 1084–1090.
49 K. Manoli, *et al.*, Printable Bioelectronics To Investigate Functional Biological Interfaces, *Angew. Chem., Int. Ed.*, 2015, **54**, 12562–12576.
50 F. Leonardi, A. Tamayo, S. Casalini and M. Mas-Torrent, Modification of the gate electrode by self-assembled monolayers in flexible electrolyte-gated organic field effect transistors: work function *vs.* capacitance effects, *RSC Adv.*, 2018, **8**, 27509–27515.
51 Q. Zhang, A. Tamayo, F. Leonardi and M. Mas-Torrent, Interplay between Electrolyte-Gated Organic Field-Effect Transistors and Surfactants: A Surface Aggregation Tool and Protecting Semiconducting Layer, *ACS Appl. Mater. Interfaces*, 2021, **13**, 30902–30909.
52 O. Livnah, E. A. Bayert, M. Wilchekt and J. L. Sussman, Three-dimensional structures of avidin and the avidin-biotin complex, *Proc. Natl. Acad. Sci. U. S. A.*, 1993, **90**(11), 5076–5080.

53 P. Strzelczyk, D. Plażuk, J. Zakrzewski and G. Bujacz, Structural characterization of the avidin interactions with fluorescent pyrene-conjugates: 1-biotinylpyrene and 1-desthiobiotinylpyrene, *Molecules*, 2016, **21**, 1270.
54 G. Palazzo, *et al.*, Detection Beyond Debye's Length with an Electrolyte–Gated Organic Field–Effect Transistor, *Adv. Mater.*, 2015, **27**, 911–916.
55 R. J. McMahon, *Avidin-Biotin Interactions: Methods and Applications*, Humana press, Totowa (N.J.), 2008.
56 S. Wang, *et al.*, Avidin–Biotin Technology in Gold Nanoparticle-Decorated Graphene Field Effect Transistors for Detection of Biotinylated Macromolecules with Ultrahigh Sensitivity and Specificity, *ACS Omega*, 2020, **5**, 30037–30046.
57 D. Ortiz-Aguayo, M. Bonet-San-Emeterio and M. Del Valle, Simultaneous Voltammetric Determination of Acetaminophen, Ascorbic Acid and Uric Acid by Use of Integrated Array of Screen-Printed Electrodes and Chemometric Tools, *Sensors*, 2019, **19**, 3286.
58 H. S. Magar, A. M. Fahim and M. S. Hashem, Accurate, affordable, and easy electrochemical detection of ascorbic acid in fresh fruit juices and pharmaceutical samples using an electroactive gelatin sulfonamide, *RSC Adv.*, 2024, **14**, 39820–39832.
59 S. Rantataro, L. Ferrer Pascual and T. Laurila, Ascorbic acid does not necessarily interfere with the electrochemical detection of dopamine, *Sci. Rep.*, 2022, **12**, 20225.